Travelling wave electrode optimisation for high speed electro-optic modulators using the Fourier series method

W. Boyu
X. Guangjun
J. Xiaomin

Indexing terms: Optoelectronics, Optimisation, Modulation

Abstract: The performance of Z-cut Mach–Zehnder high speed $LiNbO_3$ amplitude modulators with a CPW travelling wave electrode, has been analysed and optimally designed in detail by the Fourier series method. The effect of electrode and buffer layer thickness on the electric field distribution in the substract, effective microwave refractive index and characteristic impedance of CPW electrode, are discussed. Calculation shows that increasing the thickness of the electrode and SiO_2 buffer layer can improve the phase velocity mismatch between electric and optical waves, and the drive power required by the modulator with thin buffer layer and thick electrode is lower than that required by the modulator with thick buffer layer and thin electrode. In the optimisation procedure the graphic method without iteration is used with the help of a software called 'GRAPH'. The optimum rate of electrode width with gap is near by 0.75 and is independent of the rate of electrode thickness with gap. The on/off voltage lower than 4.1 V is achieved by a modulators with electrode length 59 mm for 18 GHz bandwidth.

1 Introduction

High speed optical waveguide $LiNbO_3$ electro-optic modulators are important devices for rapid developing broadband optical fibre communications and signal processing systems. Various types of high speed modulators have been developed; among them the Mach–Zehnder interferometric type modulator is one of the most widely used structures for high speed modulation, because of its simplicity and easy fabrication. In a typical broadband $LiNbO_3$ modulator, the electrode length is limited by phase velocity mismatch between the electric wave and optical wave, as well as the microwave attenuation of the travelling wave electrode. The required driven power increases with modulation bandwidth. It has prevented their practical use. In order to broaden the bandwidth and reduce the driven power, it is necessary to increase the electrode length, eliminate the velocity mismatch and reduce the microwave attenuation. Various approaches to achieve velocity match have been reported, such as phase reversal [1], shielding plane [2, 3], thickening electrode [4, 5] and application of a buried travelling wave electrode [6]. Out of these, the thickening electrode and buffer layer is the best way because of its easy fabrication. According to our experimental results and Reference 7, the coplanar waveguide (CPW) electrode is superior to the coplanar strip electrode (CPS) in the microwave transmission properties for broadband modulators. Various computational methods for calculating the electric field distribution in the integrated optics devices, such as the Fourier series [8, 9], Green's function [10, 11] and the finite element method [12, 13], have been reported. The Fourier series method has the advantage of easy division subregions and no iterations required. The purpose of this paper is to present the detailed mathematical derivation for CPW structure based on Fourier series method [9] as well as analytical results and useful design data for the $LiNbO_3$ Mach–Zehnder interferometric modulators with CPW electrode (Fig. 1 is the cross-section of the device). In this approach the impact of the

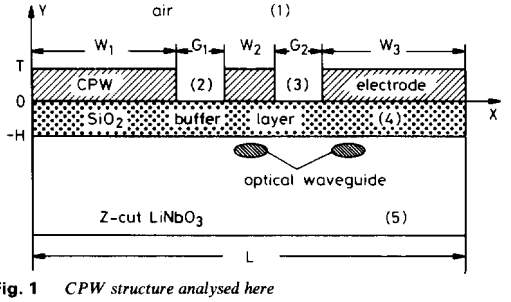

Fig. 1 *CPW structure analysed here*

geometrical parameters including finite metal and buffer layer thickness of the modulators on effective microwave refractive index, characteristic impedance and electro-optic overlap integral between electric wave and optical wave are evaluated. Furthermore, the optical small signal bandwidth, on/off voltage and required drive power of devices are calculated. The definition of the optimum

Paper 1437J (E13), first received 1st December 1993 and in revised form 13th June 1994

The authors are at the Tsinghua University, Department of Electrical Engineering, Beijing 100084, People's Republic of China

This project was supported by high technology 863 plan, China. We are indebted to the referees for some valuable comments.

design is that the modulator requires a minimum drive power for a given bandwidth. The calculated effective microwave refractive index and impedance are presented as a function of central electrode width to gap ratio W/G at various electrode thickness to gap ratio T/G and buffer layer thickness to gap ratio H/G.

2 Fourier series method for quasistatic analysis of travelling wave CPW electrode

In the integrated electro-optic modulators, the transverse dimensions of CPW electrode are much smaller than the wavelength of the travelling wave applied to the electrode. Hence, the transverse distribution of electric field in the modulators can be found by quasistatic analysis through two dimension Laplace equation and boundary conditions. The exact results have been solved by using the conformal mapping method with the infinitely thin metal electrode thickness in the modulator without the buffer layer [14]. However, this assumption is not suitable to analyse the high speed travelling wave modulator with thick metal electrode and buffer layer. The effect of the finite metal and buffer layer thickness on the characteristic impedance, effective microwave refractive index, on/off voltage, drive power and bandwidth of the high speed modulator must be analysed numerically. Among the suitable numerical methods [8–13] for analysing the structure shown in Fig. 1, Fourier series method is a simpler one.

In Fig. 1, an intermediate SiO_2 buffer layer of thickness H is deposited on top of the anisotropic substrate, then three electrodes of thickness T are deposited on top of the buffer layer. As the change in the dielectric constant due to Ti diffusion used in the fabrication of optical channel waveguide is rather small, its effect is neglected in the analysis. The substrate is assumed to be a homogeneous anisotropic dielectric with its principal dielectric axis line up along the x and y direction, which correspond to X and Z directions, respectively, in the analysis of Z-cut $LiNbO_3$ crystal. The corresponding dielectric constants are ε_x and ε_y, respectively. The buffer layer is a homogeneous isotropic dielectric of dielectric constant ε_b. Three electrodes of CPW are assumed to be perfectly conductive with rectangular shapes. The width of the central narrow electrode is W_2 and other are of W_1 and W_3 which are much wider than W_2. G_1 and G_2 are the gaps between both electrodes. The potentials applied on each electrode are V_1, V_2 and V_3, respectively. In the calculation, both side electrode are grounded with $V_1 = V_2 = 0$ and the central electrode is a hot electrode with $V_2 = 1$ V. It is assumed that there are two infinite perfectly conducting planes at $x = 0$ and $x = W_1 + G1 + W_2 + G_2 + W_3$, respectively.

Static electric field $\vec{E}$ in the structure can be expressed in terms of a potential function Φ as follows:

$$\vec{E}(x, y) = -\nabla\Phi(x, y) \tag{1}$$

We used the same method mentioned in Reference 9, which analyses the CPS structure, to find the electric field distribution in the CPW structure. The difference between CPS and CPW is that the whole region in CPW is divided into five subregions, as shown in Fig. 1. The potential in each subregion is assigned by Φi where subscript i being the label of subregion, $i = 1, 2, 3, 4$ and 5. The potential Φi in each subregion satisfies the Laplace equation, as follows:

$$\frac{\partial^2\Phi_i}{\partial x^2} + \frac{\partial^2\Phi_i}{\partial y^2} = 0 \quad i = 1, 2, 3, 4$$

$$\varepsilon_x \frac{\partial^2\Phi_i}{\partial x^2} + \varepsilon_y \frac{\partial^2\Phi_i}{\partial y^2} = 0 \quad i = 5 \tag{2}$$

The potential Φ is expanded in terms of the Fourier series, satisfying the Laplace eqn. 2 and the boundary conditions on the interfaces in the x direction:

$$\Phi_1 = \sum_{n=1}^{\infty} a_n \exp\left[-n\frac{\pi}{L}(y - T)\right] \sin\left(n\frac{\pi}{L}x\right)$$

$$\Phi_2 = V_1 + \frac{(V_2 - V_1)}{G_1}(x - W_1) + \sum_{n=1}^{\infty}\left\{b_n \exp\left[-n\frac{\pi}{G_1}(T - y)\right] + c_n \exp\left[-n\frac{\pi}{G_1}y\right]\right\} \sin\left[n\frac{\pi}{G_1}(x - W_1)\right]$$

$$\Phi_3 = V_2 + \frac{(V_3 - V_2)}{G_2}(x - W_1 - G_1 - W_2) + \sum_{n=1}^{\infty}\left\{d_n \exp\left[-n\frac{\pi}{G_2}(T - y)\right] + e_n \exp\left[-n\frac{\pi}{G_2}y\right]\right\} \times \sin\left[n\frac{\pi}{G_2}(x - W_1 - G_1 - W_2)\right]$$

$$\Phi_4 = \sum_{n=1}^{\infty}\left[f_n \exp\left(n\frac{\pi}{L}y\right) + g_n \exp\left(-n\frac{\pi}{L}y\right)\right] \times \sin\left(n\frac{\pi}{L}x\right)$$

$$\Phi_5 = \sum_{n=1}^{\infty} s_n \exp\left(n\frac{\pi}{L}ky\right) \sin\left(n\frac{\pi}{L}x\right) \tag{3}$$

where

$$k = \sqrt{(\varepsilon_x/\varepsilon_y)}$$

A set of linear equations for the eight unknown coefficients a_n, b_n, c_n, d_n, e_n, f_n, g_n, s_n in the potential expansion series (eqn. 3) can be established employing the boundary conditions on the interfaces in the y direction. Coefficients b_n, c_n, d_n, e_n, f_n, g_n are represented by a_n and s_n as follows:

$$b_n = -\frac{2}{nL\left[1 - \exp\left(-\frac{2n\pi T}{G_1}\right)\right]} \times \left[\sum_{m=1}^{\infty} mBC(n, m)a_m + \varepsilon_b \exp\left(-\frac{2n\pi T}{G_1}\right) \times \sum_{m=1}^{\infty} mFG_m BC(n, m)s_m\right]$$

$$c_n = -\frac{2}{nL\left[1-\exp\left(-\frac{2n\pi T}{G_1}\right)\right]} \times \left[\sum_{m=1}^{\infty} mBC(n,m)\exp\left(-\frac{2n\pi T}{G_1}\right)a_m + \varepsilon_b \sum_{m=1}^{\infty} mFG_m BC(n,m)s_m\right]$$

$$d_n = -\frac{2}{nL\left[1-\exp\left(-\frac{2n\pi T}{G_2}\right)\right]} \times \left[\sum_{m=1}^{\infty} mDE(n,m)a_m + \varepsilon_b \exp\left(-\frac{2n\pi T}{G_2}\right) \times \sum_{m=1}^{\infty} mFG_m DE(n,m)s_m\right]$$

$$e_n = -\frac{2}{nL\left[1-\exp\left(-\frac{2n\pi T}{G_2}\right)\right]} \times \left[\sum_{m=1}^{\infty} mDE(n,m)\exp\left(-\frac{2n\pi T}{G_2}\right)a_m + \varepsilon_b \sum_{m=1}^{\infty} mFG_m DE(n,m)s_m\right]$$

$$f_n = \frac{1}{2}\left(1+\frac{\varepsilon_y}{\varepsilon_b}k\right)\exp\left[-\frac{n\pi(k-1)H}{L}\right]s_n$$

$$g_n = \frac{1}{2}\left(1-\frac{\varepsilon_y}{\varepsilon_b}k\right)\exp\left[-\frac{n\pi(k+1)H}{L}\right]s_n \quad (4)$$

where

$$BC(n,m) = \begin{cases} \dfrac{\frac{n}{\pi}G_1}{\left(m\frac{G_1}{L}\right)^2 - n^2}\left\{(-1)^n \sin\left[\dfrac{m\pi(W_1+G_1)}{L}\right] - \sin\left[\dfrac{m\pi W_1}{L}\right]\right\} & mG_1 \neq nL \\ \dfrac{G_1}{2}\cos\left(\dfrac{m\pi W_1}{G_1}\right) & mG_1 = nL \end{cases}$$

$$DE(n,m) = \begin{cases} \dfrac{\frac{n}{\pi}G_2}{\left(m\frac{G_2}{L}\right)^2 - n^2} \times \left\{(-1)^n \sin\left[\dfrac{m\pi(W_1+G_1+W_2+G_2)}{L}\right] - \sin\left[\dfrac{m\pi(W_1+G_1+W_2)}{L}\right]\right\} & mG_2 \neq nL \\ \dfrac{G_2}{2}\cos\left[\dfrac{m\pi(W_1+G_1+W_2)}{G_2}\right] & mG_2 = nL \end{cases}$$

$$FG_m = \exp\left(-\frac{m\pi kH}{L}\right) \times \left[\sinh\left(\frac{m\pi H}{L}\right) + \frac{\varepsilon_y}{\varepsilon_b}k\cosh\left(\frac{m\pi H}{L}\right)\right]$$

The unknown coefficients a_n and s_n satisfy the linear equation array as follows:

$$\begin{bmatrix} [I]-[CAA] & -[CAS] \\ -[CSA] & [I]-[CSS] \end{bmatrix}\begin{bmatrix} [A] \\ [S] \end{bmatrix} = \begin{bmatrix} [RA] \\ [RS] \end{bmatrix} \quad (5)$$

where [A], [S], [RA] and [RS] are vectors with subscript i as follows:

$$[A]_i = a_i$$

$$[S]_i = s_i$$

$$[RA]_i = \frac{2}{i\pi}[V_1 - (-1)^i V_3] + \frac{2(V_2-V_1)L}{(i\pi)^2 G_1} \times \left\{\sin\left[\frac{i\pi(W_1+G_1)}{L}\right] - \sin\left[\frac{i\pi W_1}{L}\right]\right\} + \frac{2(V_3-V_2)L}{(i\pi)^2 G_2} \times \left\{\sin\left[\frac{i\pi(W_1+G_1+W_2+G_2)}{L}\right] - \sin\left[\frac{i\pi(W_1+G_1+W_2)}{L}\right]\right\}$$

$$[RS]_i = \frac{\exp\left(\frac{i\pi kH}{L}\right)}{\cosh\left(\frac{i\pi H}{L}\right) + \frac{\varepsilon_y}{\varepsilon_b}k\sinh\left(\frac{i\pi H}{L}\right)}[RA]_i \quad (6)$$

and [CAA], [CAS], [CSA] and [CSS] are matrices with subscript i, j as follows:

$$[CAS]_{ij} = -\frac{8\varepsilon_b jFG_j}{L^2}\left\{\sum_{n=1}^{\infty}[BC(n,i)BC(n,j) + DE(n,i)DE(n,j)]\frac{1}{n\left[1+\exp\left(\frac{n\pi T}{G_1}\right)\right]}\right\}$$

$$[CAA]_{ij} = -\frac{4j}{L^2}\left\{\sum_{n=1}^{\infty}[BC(n,i)BC(n,j) + DE(n,i)DE(n,j)]\frac{\cosh\left(\frac{n\pi T}{G_2}\right)}{n\sinh\left(\frac{n\pi T}{G_2}\right)}\right\}$$

$$[CSS]_{ij} = \frac{\varepsilon_b \exp\left(\frac{i\pi kH}{L}\right)FG_j}{\cosh\left(\frac{i\pi H}{L}\right) + \frac{\varepsilon_y}{\varepsilon_b}k\sinh\left(\frac{i\pi H}{L}\right)}[CAA]_{ij}$$

$$[CSA]_{ij} = \frac{\exp\left(\frac{i\pi kH}{L}\right)}{\cosh\left(\frac{i\pi H}{L}\right) + \frac{\varepsilon_y}{\varepsilon_b}k\sinh\left(\frac{i\pi H}{L}\right)}\frac{[CAS]_{ij}}{\varepsilon_b} \quad (7)$$

[I] is the unit matrix:

$$[I]_{ij} = 1 \quad i = j$$

$$[I]_{ij} = 0 \quad i \neq j \quad (8)$$

First, a_n and s_n ($n = 1, 2, \ldots, N$) are found from eqn. 5, which are truncated at the finite index N. The truncation index N depends on the calculation accuracy required.

Generally, $N \geqslant 40$ is needed. In these calculations N is 80. Then, all the other unknown coefficients b_n, c_n, d_n, e_n, g_n and f_n can be obtained from eqn. 4. Finally, the x, y components of the electric field in each subregion can be obtained from eqns. 1 and 3 as follows:

$$E_{1x} = -\frac{\pi}{L}\sum_{n=1}^{N} a_n n \exp\left[-\frac{n\pi}{L}(y-T)\right]\cos\left(\frac{n\pi}{L}x\right)$$

$$E_{1y} = \frac{\pi}{L}\sum_{n=1}^{N} a_n n \exp\left[-\frac{n\pi}{L}(y-T)\right]\sin\left(\frac{n\pi}{L}x\right)$$

$$E_{2x} = \frac{V_1 - V_2}{G_1} - \frac{\pi}{G_1}\sum_{n=1}^{N}\left\{b_n \exp\left[-\frac{n\pi}{G_1}(T-y)\right] + c_n \exp\left(-\frac{n\pi}{G_1}y\right)\right\} n \cos\left[\frac{n\pi}{G_1}(x - W_1)\right]$$

$$E_{2y} = -\frac{\pi}{G_1}\sum_{n=1}^{N}\left\{b_n \exp\left[-\frac{n\pi}{G_1}(T-y)\right] - c_n \exp\left(-\frac{n\pi}{G_1}y\right)\right\} n \sin\left[\frac{n\pi}{G_1}(x - W_1)\right]$$

$$E_{3x} = \frac{V_2 - V_3}{G_2} - \frac{\pi}{G_2}\sum_{n=1}^{N}\left\{d_n \exp\left[-\frac{n\pi}{G_2}(T-y)\right] + e_n \exp\left(-\frac{n\pi}{G_2}y\right)\right\} n \times \cos\left[\frac{n\pi}{G_2}(x - W_1 - G_1 - W_2)\right]$$

$$E_{3y} = -\frac{\pi}{G_2}\sum_{n=1}^{N}\left\{d_n \exp\left[-\frac{n\pi}{G_2}(T-y)\right] - e_n \exp\left(-\frac{n\pi}{G_2}y\right)\right\} n \times \sin\left[\frac{n\pi}{G_2}(x - W_1 - G_1 - W_2)\right]$$

$$E_{4x} = -\frac{\pi}{L}\sum_{n=1}^{N}\left[f_n \exp\left(\frac{n\pi}{L}y\right) + g_n \exp\left(-\frac{n\pi}{L}y\right)\right] n \cos\left(\frac{n\pi}{L}x\right)$$

$$E_{4y} = -\frac{\pi}{L}\sum_{n=1}^{N}\left[f_n \exp\left(\frac{n\pi}{L}y\right) - g_n \exp\left(-\frac{n\pi}{L}y\right)\right] n \sin\left(\frac{n\pi}{L}x\right)$$

$$E_{5x} = -\frac{\pi}{L}\sum_{n=1}^{N} s_n \exp\left(\frac{n\pi}{L}ky\right) n \cos\left(\frac{n\pi}{L}x\right)$$

$$E_{5y} = -\frac{\pi}{L}k\sum_{n=1}^{N} s_n \exp\left(\frac{n\pi}{L}ky\right) n \sin\left(\frac{n\pi}{L}x\right) \quad (9)$$

3 Formula for modulator analysis

3.1 Characteristic impedance Zm and effective microwave refractive index Nm

Zm and Nm are two important parameters in the design of travelling wave modulators. They affect the impedance match between the electrodes and driving circuit, and hence the modulation bandwidth. For any TEM-type transmission line, the Zm and Nm at microwave frequencies can be found by the x, y components of the electric field E which were given in eqn. 9 [10].

3.2 Drive power requirement

The drive power required by a M–Z modulator for completely switching at modulation frequency f is defined as the available power from a microwave source with impedance $Zs = 50\ \Omega$ and can be written as

$$P_{dr}(f) = \frac{1}{8Zs}\left[\frac{(Zm + Zs)V_\pi}{2ZmH(f)}\right]^2 = \frac{P_{dr}}{H^2(f)} \quad (10)$$

where

$$V_\pi = \frac{\lambda G}{r_{33} n_e^3 \Gamma L} \quad (11)$$

where G is the gap between both electrodes on each optical channel waveguide, L is the electrode length, λ is the optical wavelength, r_{33} and n_e are the electro-optic coefficient and the optical refractive index of $LiNbO_3$ crystal, respectively.

$H(f)$ is the frequency response function [10]. At high modulation frequencies when the dielectric loss in the substrate and SiO_2 buffer layer are negligible, α can be written as [16, 17]

$$\alpha = \alpha_0\sqrt{(f)} \quad (12)$$

In the following calculations we use the approximative formula of α_0 in Reference 17.

In Fig. 2, the contour lines of the electrode length for a travelling wave modulator with 18 GHz bandwidth are

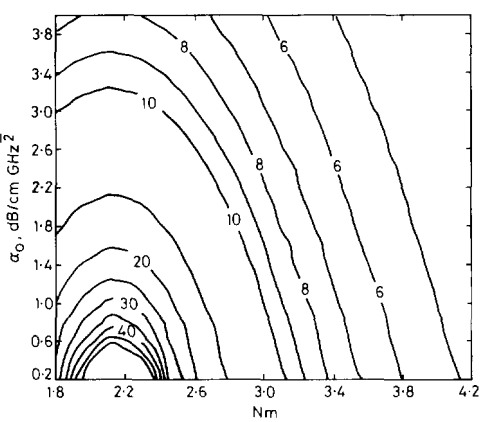

Fig. 2 *Contour lines of the electrode length L mm as the function of Nm and α_0 for the bandwidth of 18 GHz*

plotted in the Nm-α_0 plane. It is noted that the maximum electrode length is achieved at $Nm = n_e = 2.138$ for a given α_0.

$\Gamma = \Gamma_1 - \Gamma_2$ is the total overlap integral of a M–Z modulator. The overlap integral on each optical channel waveguide is

$$\Gamma_i = \frac{G\int_{-\infty}^{\infty}\int_{-\infty}^{\infty} E_{0i}^2(x, y)E_e(x, y)\,dx\,dy}{\int_{-\infty}^{\infty}\int_{-\infty}^{\infty} E_{0i}^2(x, y)\,dx\,dy} \quad (i = 1, 2) \quad (13)$$

where $E_e(x, y)$ is the microwave electric field per unit voltage applied on the electrode. $E_{0i}(x, y)$ is the electric field pattern of the optical wave of the ith arm and is assumed as electric field with Gaussian and Hermite–Gaussian distribution in x and y direction, respectively,

and is expressed as follows [15]:

$$E_{0i}(x, y) = E_{0ix}(x)E_{0i}(y) \tag{14}$$

where

$$E_{0ix}(x) = \frac{\exp\left\{-\frac{1}{2}\left[\frac{2(x-x_i)}{W_0}\right]^2\right\}}{\sqrt{\left(\frac{W_0\sqrt{(\pi)}}{2}\right)}} \tag{15}$$

$$E_{0i}(y) = \frac{2y\exp\left[-\frac{1}{2}\left(\frac{y}{d}\right)^2\right]}{d\sqrt{[d\sqrt{(\pi)}]}} \tag{16}$$

$$W_0 = \frac{W_{\|}}{\sqrt{(2)}} \tag{17}$$

$$d = 0.528125W_{\perp} \tag{18}$$

x_i is the x coordinate of the centre of the optical channel waveguide on ith arm of a M–Z modulator. $W_{\|}$ and $W_{\perp}$ are the full widths at $1/e$ the maximum values of the horizontal and vertical electric field patterns of the optical wave, respectively. When the optical channel waveguides on the arms are as same as the channel waveguides at input and output parts of the M–Z modulator, to achieve the minimum coupling loss between optical waveguide and optic fibre. $W_{\|}$, $W_{\perp}$ and $2a$ must satisfy the following relation:

$$(2a)^2 = W_{\|}\,W_{\perp} \tag{19}$$

where $2a$ is the mode field diameter of the circle symmetric single mode fibre. In the following analysis of the modulator, $2a$ can be regarded as a constant depending on the single mode fibre type at required optic wavelength.

Eqn. 10 shows that the maximum drive power in the bandwidth from DC to f_{s0} is $4P_{dr}$ at f_{s0}. In the following analysis, the P_{dr} will be an important final parameter.

4 Comparison to an exact solution of electric field and the experimental results of some modulators

4.1 Comparison of electric field

Although the conformal mapping method is not suitable for analysing the structure with finite metal electrode and buffer layer, the field solution [14] is exact for a structure where the electrodes are assumed to be infinitely thin and both side electrodes to be semi-infinite at transverse direction. Therefore, the electric field distribution calculated by the Fourier series method can be compared with that calculated by the conformal mapping method in order to determine accuracy of Fourier series method.

Fig. 3 shows the electric field $E_x(x)$ and $E_y(x)$ in the x and y direction in the substrate as a function of x for $y = -5$ μm and $H = 0$. Generally, the maximum of optical field pattern is near to $y = -5$ μm. The substrate is Z-cut $LiNbO_3$ crystal with $\varepsilon_x = 43$ and $\varepsilon_y = 28$. The electrode dimensions are $W_2 = 8$ μm, $W_1 = W_3 = 100$ μm, $G_1 = G_2 = 15$ μm and $T = 0.01$ μm. In the Fourier series method, the T value cannot be zero, and $T = 0.01$ μm is much less than G_1 and W_2. V_2 and $V_1 = V_3$ are assumed to be of 1 V and 0 V, respectively. The solid line represents the exact solution of conformal mapping method (CMM) while the dashed lines represent the results of the Fourier series method (FSM). As Fig. 3 shows, the field distributions calculated by both methods are in very good agreement. At $x = W_1 + G_1 + W_2/2 = 119$ μm (see Fig. 1), the E_y reaches its maximum and the relative error of the electric field is only 1.4%.

4.2 Comparison to the experimental results

The accuracy of electric field calculated by Fourier series method affects the accuracy of calculated Γ, V_π, N_m, Z_m, P_{dr} and bandwidth of the modulator with thick metal electrode and thick buffer layer. Thus, a comparison between the theoretical calculations and the experimental results of some CPW travelling wave modulators is very important to see whether the Fourier series method is good for an engineering design of the modulator. Table 1 is the comparison and shows that the relative error of V_π and 3 dB bandwidth BW are less than 9% and 5%, respectively.

It is evident from the above comparison that the Fourier series method is accurate not only in the special case of the infinitely thin electrodes without buffer layer, but also in the general case of electrode and buffer layer with finite thickness. Thus it has been demonstrated to be useful for the analysis and engineering design of CPW $LiNbO_3$ M–Z modulators.

5 Calculations

In this section we will analyse the effects of the electrode thickness T and buffer layer thickness H on the electric fields in the substrate, the characteristic impedance Z_m and the effective microwave refractive index N_m. In the following calculations, W and G represent W_2 and $G_1 = G_2$ in Fig. 1, respectively. The $y = 0$ plane lies at the interface between the SiO_2 buffer layer and electrodes.

5.1 Electric field distribution

In Fig. 4, the electric field E_x and E_y are plotted as a function of $x' = x - 119$ μm for various electrode thick-

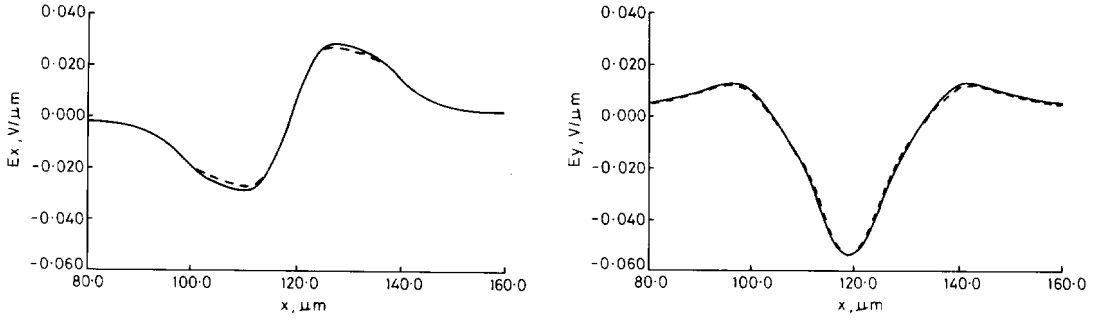

Fig. 3 *Comparison of the field distribution calculated by conformal mapping method (CMM) and Fourier series method (FSM) at $y = -5$ μm*

nesses, with $W = 8\ \mu m$, $G = 15\ \mu m$ and $H = 0.5\ \mu m$ at $y' = y - H = -10\ \mu m$ under the bottom of buffer layer. It is shown that the electric field distribution is nearly unvaried when the electrode thickness increases from 3 μm to 12 μm. This means that increasing electrode thickness does not lead to an increase of V_π, and is very useful in the optimum design of the modulator.

Fig. 5 shows the electric field distribution for various buffer layer thickness with $W = 8\ \mu m$, $G = 15\ \mu m$, $T = 3\ \mu m$ at $y' = -10\ \mu m$. It is noted that the shapes of the field distribution are nearly unchanged, but the values of the electric field at the same x' obviously decrease when the buffer layer thickness increases from 0 to 3 μm. As H increases from 0.5 to 1 μm it makes a 23.5% reduction in the value of the electric field. This means that V_π required by the modulator will increase.

5.2 Characteristic impedance Z_m and effective microwave refractive index N_m

Fig. 6 shows Z_m and N_m as a function of T/G for various values of H/G with $W/G = 0.5$. Fig. 7 shows Z_m and N_m as a function of H/G for various values of W/G with $T/G = 0.2$. It is observed from Figs. 6 and 7 that N_m decreases as T and H increase. This can be used to improve the velocity mismatch between electric and optical waves, as well as to expand the bandwidth.

6 Optimisation of Z-cut $LiNbO_3$ travelling-wave CPW M–Z modulators

Optimisation of modulator requires tradeoffs among various design parameters in order to achieve the minimum drive power required at a given bandwidth. The optimisation for given electrode thickness $T = 3\ \mu m$ [10] has been reported, but we discovered that there are a lot of very useful results for improving modulator performance in the thick electrode range ($T = 8$ to $30\ \mu m$), and the drive power of V_π required in the modulator with a thicker electrode is lower than that with a thinner electrode at a given bandwidth.

From our conformal mapping analysis of four M–Z modulators with no buffer layer and infinitely CPS or CPW thin electrodes deposited on X-cut or Z-cut $LiNbO_3$, we know that the Z-cut $LiNbO_3$ modulator is the best structure and its optimum gap $G = G_1 = G_2$ is in a wide range around 18 μm. Furthermore, our experiments on optical coupling between optical channel waveguides of 28 mm length under various waveguide gaps at

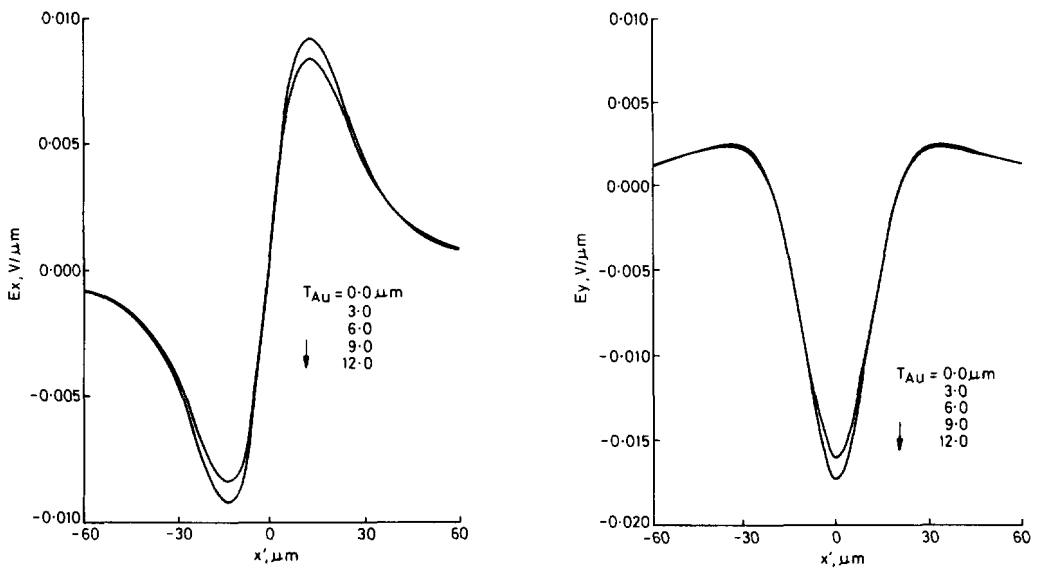

Fig. 4 *Electric field E_x and E_y as a function of $x' = x - 119\ \mu m$ for various electrode thickness with $W = 8\ \mu m$, $G = 15\ \mu m$, $H = 0.5\ \mu m$ at $y' = y - H = -10\ \mu m$ under the bottom of buffer layer*

Table 1: Comparison between calculated results by Fourier series and experimental results of Z-cut CPW modulators at $\lambda = 1.55\ \mu m$

Type	Parameter	Experimental results	Theoretical results	Relative error	Comments
[15] NTT No. 1	$W = 8$; $G = 15$	$V_\pi = 4.9$	$V_\pi = 4.95$	V_π 1%	
	$T = 4$; $H = 1.2$				$\lambda = 1.52$
	$L = 27$	BW = 8.7	BW = 9.1	BW 4.6%	
[15] NTT No. 2	$W = 8$; $G = 30$	$V_\pi = 4.4$	$V_\pi = 4.76$	V_π 8.2%	
	$T = 4$; $H = 0.45$				$\lambda = 1.52$
	$L = 20$	BW = 6.2	BW = 6.2	BW 4.8%	
[3] NRL	$W = 8$; $G = 15$	$V_\pi = 4.2$	$V_\pi = 4.28$	V_π 1.9%	
	$T = 18$; $H = 0.9$				$\lambda = 1.3$
	$L = 24$	BW = 35	BW = 34.5	BW 1.4%	

where $W = W_2$, $G = G_1 = G_2$ in Fig. 1. The unit of W, G, T, H and λ is μm. And the units of L, V_π and BW are mm, V and GHz, respectively

1.55 μm wavelength show that no optical coupling can be observed until the gap reduces to 15 μm. So that $G = 15$ μm is selected to be a basic parameter in the process of optimisation. The iteration method for optimisation [10] needs large amounts of computation time. However, in our optimisation procedure, the graphic method of separate values is used. Initially, drive powers required by the modulator with 18 GHz bandwidth are calculated at each parameter group of W/G, T/G and H/G. The electrode length is assumed to be unlimited.

The TM mode size $W_{\|}$ and $W_{\perp}$ in eqns. 17 and 18 are dependent on the waveguide fabrication conditions. In our laboratory the channel waveguides on Z-cut $LiNbO_3$ are fabricated by T_i indiffusion technology at 1050°C diffusion temperature, for 9 h diffusion time in a wet oxygen atmosphere. The T_i stripe is 85 nm thickness and 9–10 μm width. At 1.55 μm wavelength the measured TM mode size $W_{\|}$ and $W_{\perp}$ are 14.39 and 14.56 μm, respectively. The measured optical channel waveguide propagation loss is less than 0.2 dB/cm for the 200 nm thickness SiO_2 buffer layer. The 0.1 dB/cm channel waveguide propagation loss on Z-cut $LiNbO_3$ at 1.3 μm wavelength has been reported [18]. However, the optical channel waveguide propagation loss is neglected and the TM mode sizes $W_{\|} = W_{\perp}$ are of 14 μm in the process of optimisation. Then, with the help of a software called GRAPH, the contour lines of drive power are plotted in a 2D plane with T/G as X and H/G as Y for a given W/G. The minimum drive power for each W/G can be obtained from the figure. The minimums are then plotted as a function of W/G in a figure where the optimum drive power is found.

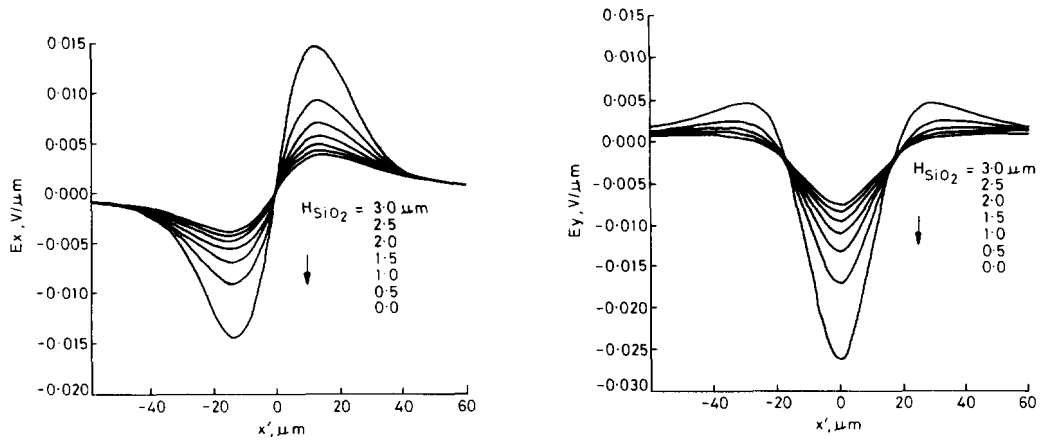

Fig. 5 *Electric field E_x and E_y as a function of $x' = x - 119$ μm for various buffer layer thickness is with $W = 8$ μm, $G = 15$ μm, $T = 3$ μm at $y' = -10$ μm*

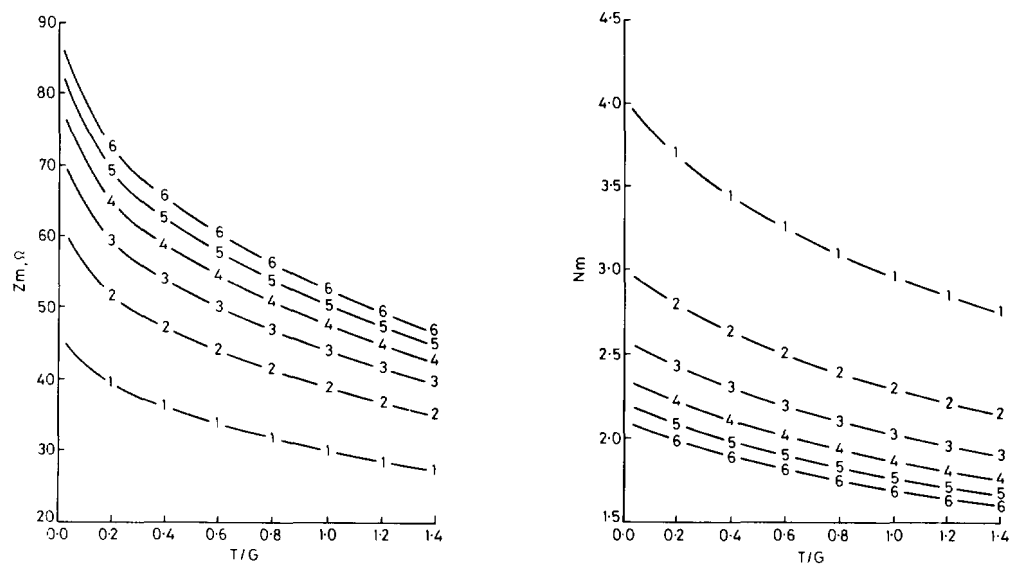

Fig. 6 *Z_m and N_m as a function of T/G for various values of H/G with $W/G = 0.5$*

1: H/G = 0.00 4: H/G = 0.15
2: H/G = 0.05 5: H/G = 0.20
3: H/G = 0.10 6: H/G = 0.25

The ranges of the selected parameters are as follows:

$4.5\ \mu m \leqslant W \leqslant 30\ \mu m \quad 0.3 \leqslant W/G \leqslant 2$

$0.15\ \mu m \leqslant T \leqslant 30\ \mu m \quad 0.01 \leqslant T/G \leqslant 2$

$0\ \mu m \leqslant H \leqslant 3.75\ \mu m \quad 0 \leqslant H/G \leqslant 0.25$

Figs. 8 and 9 show the contour lines of drive power P_{dr} in T/G–H/G plane at $G = 15\ \mu m$ for $W/G = 0.3$ and 0.75, respectively. Fig. 10 is the required minimum drive power value as a function of W/G for $T/G = 0.6$, 0.8 and 1. It shows that the optimum range of W/G is near 0.75. In Table 2, a series of the parameters are presented corresponding to the minimum drive power required by the modulators at $W/G = 0.75$ for $G = 15\ \mu m$, $W_{\|} = W_{\perp} = 14\ \mu m$ and 18 GHz bandwidth. These data are useful for design of CPW $LiNbO_3$ M–Z modulators in taking practical conditions of the fabrication process and equipment into account.

It is known from eqns. 10, 11 and 13–18, that V_{π} and P_{dr} are depended on the $W_{\|}$ and $W_{\perp}$. Low drive power is obtained by small TM mode size $W_{\|}$ and $W_{\perp}$ which depend on optical waveguide fabrication conditions. When the optical waveguides in the arms are different with the waveguides in input and output parts in a M–Z modulator, $W_{\|}$ and $W_{\perp}$ are not limited by eqn. 19. For example, in $G = 15\ \mu m$, $L = 59.3$ mm, $T/G = 1.6$, $H/G = 0.0624$, M–Z modulator whose electrode configuration is same as the fifth row data in Table 2, $V_{\pi} =$

Table 2: Parameters corresponding to minimum drive power required by the modulators at $W/G = 0.75$ for $G = 15\ \mu m$, $W_{\perp} = W_{\|} = 14\ \mu m$ and 18 GHz bandwidth

T/G	H/G	N_m	Z_m (Ω)	L (mm)	V_{π} (V)	P_{dr} (W)	$V_{\pi}L$ (V mm)
0.8	0.1200	2.159	42.83	42.256	8.01	0.1883	338.5
1.0	0.1020	2.150	39.16	44.323	6.94	0.1561	307.6
1.2	0.0866	2.145	36.03	47.288	5.94	0.1259	271.4
1.4	0.0732	2.142	33.32	51.864	4.97	0.0965	257.8
1.6	0.0624	2.139	31.03	59.325	4.02	0.0690	238.5
1.8	0.0546	2.127	29.15	71.741	3.13	0.0452	224.5
2.0	0.0499	2.105	27.64	88.895	2.43	0.0290	216.0

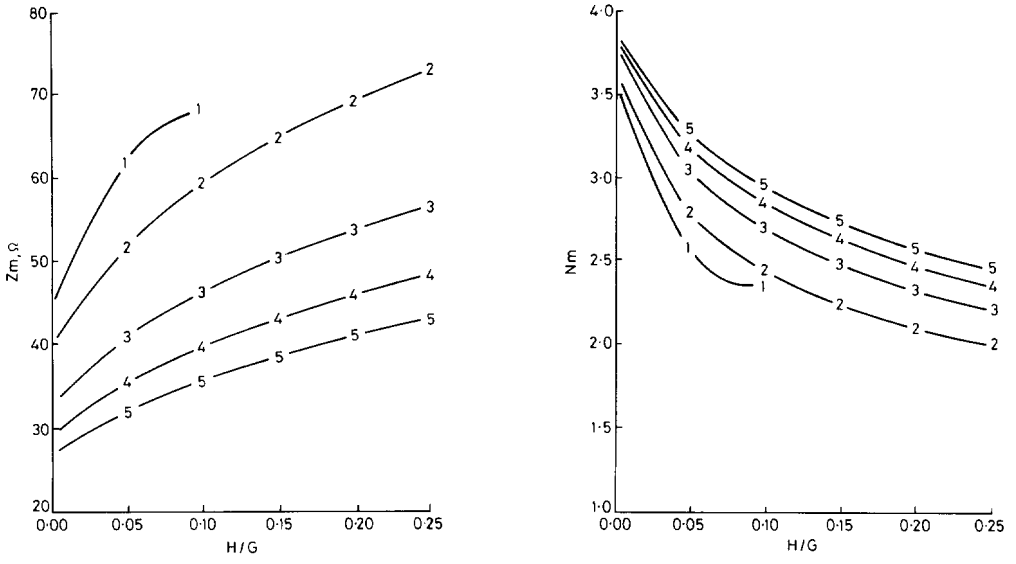

Fig. 7 *Z_m and N_m as a function of H/G for various values of W/G with $T/G = 0.2$*
1: W/G = 0.3 4: W/G = 1.5
2: W/G = 0.5 5: W/G = 2.0
3: W/G = 1.0

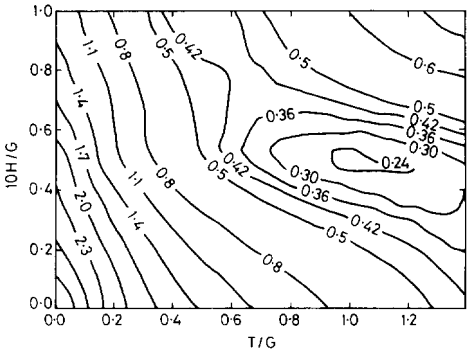

Fig. 8 *Equal value curves of drive power P_{dr} in T/G–H/G plane at $G = 15\ \mu m$ for $W/G = 0.3$*

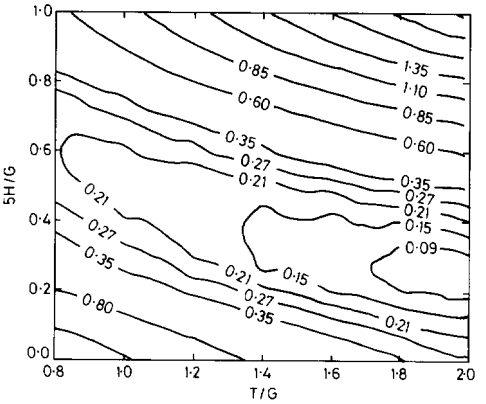

Fig. 9 *Equal value curves of drive power in T/G–H/G plane for $W/G = 0.75$*

2.38 V and $P_{dr} = 0.024$ W can be obtained for the experimental TM mode size $W_{\|} = 9.51$ μm and $W_{\perp} = 7.38$ μm corresponding to the full-width half-maximum (FWHM) intensity of 5.6 μm lateral by 4.5 μm vertical [15] at

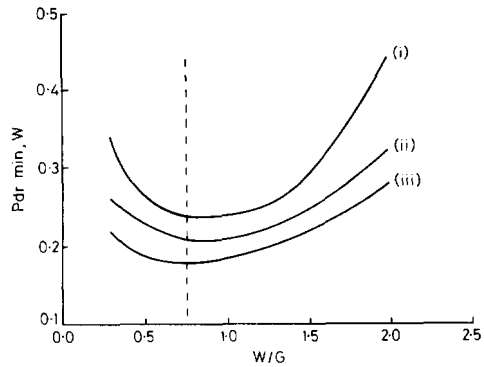

Fig. 10 *Minimum drive power required for $T/G = 0.6$, 0.8 and 1 as the functions of W/G*
(i) T/G = 0.6
(ii) T/G = 0.8
(iii) T/G = 1.0

1.3 μm wavelength. If the calculated TM mode size $W_{\|} = 4.47$ μm and $W_{\perp} = 5.61$ μm (corresponding to FWHM intensity of 2.63 μm lateral by 3.42 μm [10]) can be realised in the channel waveguide at 1.3 μm wavelength, there is no doubt that the lower on/off voltage $V_{\pi} = 1.98$ V and drive power $P_{dr} = 0.0166$ W are very attractive.

7 Discussion

1. Increasing the electrode thickness T of the modulator with a given buffer layer thickness H improves the velocity mismatch between optical and electric waves, because the effective microwave refractive index N_m is near to the optical refractive index n_e. It also reduces the microwave propagating attenuation constant which does not change the electric field intensity in the substrate and the electro-optical integral Γ. Therefore, the electrode length L limited by the given bandwidth can be expanded to achieve lower on/off voltage. But, as continually increasing electrode thickness, N_m becomes less than n_e, and the velocity mismatch occurs as the required drive power increases, so that there is an optimum electrode thickness.

2. Generally speaking, increasing the buffer layer thickness H with a given electrode thickness T also can improve the velocity match and leads to an increase of the characteristic impedance and a reduction of the microwave attenuation constant. One can use longer electrode length to compensate the effect of decreasing electric field in the optical channel waveguide in order to reduce the drive power; but, as the electrode thickness is thinner, the buffer layer thickness required by getting the velocity match becomes thicker, which rapidly decrease the electric field intensity in the optical waveguide, so that the minimum drive power obtained by increasing buffer layer thickness H with thin electrode is higher than that obtained by increasing electrode thickness T with thin buffer layer. The optimum drive power is found at $T/G = 2$ ($T = 30$ μm) and $H/G = 0.05$ ($H = 0.75$ μm) in our selective range. In this case, the electrode length and DC on/off voltage are 88.9 mm and 2.43 V, respectively, and the required drive power at 18 GHz is 0.116 W.

3. Fig. 10 shows that the drive power as a function of W/G slowly varies at near $W/G = 0.75$. This means that the tolerance of the electrode width W and gap G in fabricating modulators has only a slight influence on the drive power.

8 Conclusion

In this paper, the Fourier series method used to calculate the quasistatic electric field distribution in CPW Z-cut $LiNbO_3$ modulators with the finite electrode and buffer layer thickness has been described in detail. The comparison theoretical calculation with experimental results proves that the calculated performance of the modulator by using the Fourier series method is accurate enough for engineering design.

In order to achieve the optimum drive power required by the modulator trade-offs among various parameters of the structure is treated by the graphic method without iteration. When the electrode length L is assumed to be unlimited, a lot of separate values of drive power are calculated from varying electrode widths W, thicknesses T and buffer layer thicknesses H for a given gap G and optical small signal bandwidth. The graph of contour line of drive power as a function of T/G, H/G for various W/G is plotted with the help of a software called GRAPH. The minimum drive power required by the modulators is shown on the graphs. In Table 2, the data are presented for 18 GHz modulator with $G = 15$ μm.

Calculation shows that increasing both electrode and buffer layer thickness can improve the velocity mismatch between optical and electric waves. Consequently, it is promising to increase the electrode length, hence decrease on/off voltage and drive power for a given bandwidth. The drive power required by the modulator with thin buffer layer and thick electrode is lower than that required by the modulator with thick buffer layer and thin electrode. The optimum rate W/G of electrode width with gap is near by 0.75 and independent of the rate T/G of electrode thickness with gap. Meanwhile the general curve groups of the characteristic impedance Z_m and effective microwave refractive index N_m of CPW as a function of the parameters T/G, H/G and W/G have been presented.

9 References

1 DOLFI, D.W., and NAZARATHY, M.: '40 GHz electro-optic modulator with 7.5 V drive voltage', *Electron. Lett.*, 1988, **24**, (9), pp. 528–529
2 KAWANO, K., KITOH, T., JUMONJI, H., NOZAWA, T., and YANAGIBASH, M.: 'New travelling wave electrode Mach–Zehnder optical modulator with 20 GHz bandwidth and 4.7 V driving voltage at 1.52 μm wavelength', *Electron. Lett.*, 1989, **25**, (20), pp. 1382–1383
3 NOGUCHI, K., and KAWANO, K.: 'Proposal for Ti : $LiNbO_3$ optical modulator with modulation bandwidth of more than 150 GHz', *Electron. Lett.*, 1992, **28**, (18), pp. 1759–1761
4 KAWANO, K., KITOH, T., JUMONJI, H., NOZAWA, T., YANAGIBASHI, M., and SUZUKI, T.: 'Spectral-domain analysis of coplanar waveguide traveling-wave electrodes and their application to Ti : $LiNbO_3$ Mach–Zehnder optical modulators', *IEEE Trans.*, 1991, **MTT-39**, (9), pp. 1595–1601
5 GOPALAKRISHNAN, G.K., BULMER, C.H., BURNS, W.K., McELHANON, R.W., and GREENBLATT, A.S.: '40 GHz low half-wave voltage Ti : $LiNbO_3$ intensity modulator', *Electron. Lett.*, 1992, **28**, (9), pp. 826–827
6 OHTA, H., MIYAMOTO, H., TABUSE, K., and MIYAGAWA, Y.: 'Ti : $LiNbO_3$ Mach–Zehnder modulator using a buried traveling wave electrode'. 1992 Technical Digest of Optical Fiber Communication Conference, paper ThG3
7 GOPALAKRISHNAN, G.K., BURNS, W.K., and BULMER, C.H.: 'Electrical loss mechanisms in traveling wave $LiNbO_3$ optical modulators', *Electron. Lett.*, 1992, **28**, (2), pp. 207–208

8 MARCUSE, D.: 'Electrostatic field of coplanar line computed with the point matching method', *IEEE J. Quantum Electron.*, 1989, **25**, (5), pp. 939–947
9 JIN, H., BELANGER, M., and JALCUBCZYK, Z.: 'General analysis of electrodes in integrated optics electrooptic devices', *IEEE J. Quantum Electron.*, 1991, **27**, (2), pp. 243–251
10 CHUNG, H., CHANG, W.S.C., and ADLER, E.L.: 'Modeling and optimization of traveling-wave $LiNbO_3$ interferometric modulators', *IEEE J. Quantum Electron.*, 1991, **27**, (3), pp. 608–617
11 RAILTON, C.J., and McGEEHAN, J.P.: 'A rigorous and computationally efficient analysis of microstrip for use as an electro-optic modulator', *IEEE Trans.*, 1989, **MTT-37**, (7), pp. 1099–1103
12 YI, J.C., KIM, S.H., and CHOI, S.S: 'Finite-element method for the impedance analysis of traveling wave modulators', *J. Lightwave Technol.*, 1990, **8**, (6), pp. 817–822
13 DAVIDOVITZ, M., WU, Z., and GOPINATH, A.: 'Analysis of electrooptic device electrodes: influence of metalization thickness, substrate optical axis inclination and buffer layer'. 1992 Technical Digest of Integrated Photonics Research, New Orleans, United States of America, paper MB16 1–4
14 RAMER, O.G.: 'Integrated optic electrooptic modulator electrode analysis', *IEEE J. Quantum Electron.*, 1982, **QE-18**, (3), pp. 386–392
15 KOROTKY, S., MINFORD, W.J., BUHL, L.L., DIVINO, M.D., and ALFERNESS, R.C.: 'Mode size and method for estimating the propagation constant of single-mode Ti : $LiNbO_3$ strip waveguides', *IEEE J. Quantum Electron.*, 1982, **QE-18**, (10), pp. 1796–1801
16 DONNELLY, J.P., and GOPINATH, A.: 'A comparison of power requirements of traveling wave $LiNbO_3$ optical couplers and interferometric modulators', *IEEE J. Quantum Electron.*, 1987, **QE-23**, (1), pp. 30–41
17 CHUNG, H., and CHANG, W.S.C.: 'Optimization of microwave frequency traveling-wave $LiNbO_3$ integrated-optic modulators'. PhD thesis, 1990, University of California, San Diego, USA, pp. 49–55
18 KOMATSU, K., YAMAZAKI, S., KONDO, M., and OHTA, Y.: 'Low-loss broad-band $LiNbO_3$ guided-wave phase modulators using titanium/magnesium double diffusion method', *J. Lightwave Technol.*, 1987, **LT-5**, (9), pp. 1239–1245